https://doi.org/10.2514/1.J058322
AIAA JOURNAL, Vol. 58, No. 12, pp.5107-5116, December 2020

Propulsion Performance of Cylindrical Rotating Detonation Engine

Ryuya Yokoo,[*] Kesisuke Goto,[†] Juhoe Kim,[‡] Akira Kawasaki,[§] Ken Matsuoka[**] and Jiro Kasahara[††]
Nagoya University, Nagoya, Aichi, 464-8603, Japan

Akiko Matsuo[‡‡]
Keio University, Yokohama, Kanagawa, 223-8522, Japan

and
Ikkoh Funaki[§§]
Japan Aerospace Exploration Agency, Sagamihara, Kanagawa, 252-5210, Japan

We evaluated the propulsion performance of a nozzleless, cylindrical rotating detonation engine (RDE). Using a C_2H_4–O_2 mixture, the RDE was tested in a low-back-pressure environment at propellant mass flow rates of 8–45 g/s. In high-speed imaging of the self-luminescence within the combustor, rotating luminous regions were observed at mass flow rates above 22 g/s. Measured pressure distributions suggest that burned gas reached sonic velocity at the combustion chamber outlet. We propose the structure of internal flow in the RDE, and confirm that calculated pressure distribution based on the structure was close to the experimental distribution. We also estimated the RDE's thrust by pressure and momentum exchange and confirmed it by experimental measurement. Moreover, the theoretical thrust calculated under the assumption that exhaust is a sonic flow agreed with the load cell thrusts, suggesting that RDE combustion is perfectly completed inside the chamber. Specific impulse exceeded 80% of specific impulse of correct expanded for all mass flow rates, and its value was close to that of an annular RDE. In addition, RDE performance will increase

[*] Graduate Student, Department of Aerospace Engineering, Nagoya, Aichi, 464-8603, Japan, Student Member AIAA
[†] Doctoral Student, Department of Aerospace Engineering, Nagoya, Aichi, 464-8603, Japan, Student Member AIAA
[‡] Undergraduate Student, Department of Aerospace Engineering, Nagoya, Aichi, 464-8603, Japan
[§] Assistant Professor, Department of Aerospace Engineering, Nagoya, Aichi, 464-8603, Japan, Member AIAA
[**] Associate Professor, Department of Aerospace Engineering, Nagoya, Aichi, 464-8603, Japan, Member AIAA
[††] Professor, Department of Aerospace Engineering, Nagoya, Aichi, 464-8603, Japan, Associate Fellow AIAA
[‡‡] Professor, Department of Mechanical Engineering, Yokohama, Kanagawa, 223-8522, Japan, Senior Member AIAA
[§§] Professor, Institute of Space and Astronautical Science, Sagamihara, Kanagawa, 252-5210, Japan, Senior Member AIAA

https://doi.org/10.2514/1.J058322
AIAA JOURNAL, Vol. 58, No. 12, pp.5107-5116, December 2020

by about 20% if the RDE is equipped with a divergent nozzle and the gas is correctly expanded to back pressure.

Nomenclature

A_c = cross-sectional area of combustion chamber (= $\pi d_o^2/4$)

A_{inj} = the sum of cross-sectional area of injector holes

D = wave velocity of detonation

d = diameter

d_o = combustion chamber diameter

F = thrust

F_c = cold flow thrust

$\bar{F}_L$ = averaged load cell thrust of combustion duration

$F_{S,theory}$ = theoretical thrust calculated under the assumption of sonic exhaust flow

F_a = thrust calculated from pressure and momentum thrust of control surface 1

g = gravitational acceleration

L = combustion chamber length

$\dot{m}$ = mass flow rate

M_z = axial Mach number

p = pressure

p_b = back pressure

p_c = pressure of combustion at chamber bottom

p_i = pressure of chamber at z = i (i = 5, 10, 20, 30, 40, 50, 65)

R = gas constant

T = temperature

v = gas velocity

D = rotating wave velocity

z = axial position of combustion chamber

z_{rc} = axial position of chemical reaction completion

https://doi.org/10.2514/1.J058322
AIAA JOURNAL, Vol. 58, No. 12, pp.5107-5116, December 2020

γ = specific heat ratio

δ^* = displacement thickness of boundary layer

v = dynamic viscosity

ρ = density

Φ = equivalence ratio

Subscripts

c = combustion chamber

e = chamber exit

es = exit surface of chamber

p = propellant

ple = plenum

ox = oxidizer

f = fuel

z = z position

I. Introduction

DETONATION combustion involves a supersonic combustion wave propagating in a premixed fuel-oxidizer mixture [1-3]. This form of combustion features higher combustion temperature and pressure compared to deflagration combustion, and thus its thermal efficiency is theoretically higher than the Brayton cycle in conventional internal combustion engines [4]. Moreover, the burning process of detonation combustion is completed instantly due to the supersonic combustion wave. Therefore, engines utilizing detonation combustion can realize a compact combustor with higher thermal efficiency compared to conventional engines [4-7]. It is also possible to reduce the load on the compressor, since pressure is greatly increased by the detonation wave. Wolanski [4], Kailasanath [5], Lu et al. [6], and Li et al. [7] have published comprehensive summaries of detonation propulsion applications. Rotating detonation engines (RDE) and pulse detonation engines (PDE) [8] are the well-known forms of such engines. RDEs typically have an annular combustor, and generate thrust by a detonation wave rotating in the circumferential direction. RDEs can usually exert higher thrust densities than PDEs due to continuous combustion. Therefore, RDEs are attracting

https://doi.org/10.2514/1.J058322
AIAA JOURNAL, Vol. 58, No. 12, pp.5107-5116, December 2020

significant attention for aerospace applications such as for the main engines of rockets and airplanes, and as gas turbine engines for power generation.

Several researchers have investigated geometric parameters for stabilizing rotating detonation waves [9-11]. Bykovskii et al. [9] clarified the relation between cell size and optimal geometric conditions, such as inner radius, channel width, and combustor length, to drive RDE as a detonation engine. George et al. [10] investigated the effect of cell size and channel width on the existence of detonation waves and their number. Nakayama et al. [11] examined the influence of inner radius on the stability of detonation waves.

Prediction of RDE thrust performance has also recently been studied. Several reports suggest that thrust performance can be predicted by a control volume method and steady-state analysis on the flow field in RDE, which is originally a time-varying and high-frequency phenomenon. Wintenberger et al. [12] and Endo et al. [13] originally developed this idea for performance prediction of PDE. Rankin et al. [14] and Fotia et al. [15] then observed that the specific impulse of RDE was close to the theoretical values calculated from this model. Shepherd et al. [16] modified the PDE prediction model into a more suitable mode for RDE. Some numerical studies have also suggested steady-state analysis for RDE in order to reduce computational cost and enable parametric studies [17-18]. Fievisohn et al. [17] conducted low-cost steady-state analysis of RDE performance that considered the internal flow field by the method of characteristics. Mizener et al. [18] numerically examined RDE performance by developing a low-order performance model based on the control volume method. Others have attempted to evaluate thrust performance using methods developed for conventional rocket engines, such as quasi-one-dimensional (1-D) flow theory [19-20]. Knowlen et al. [19] introduced Rayleigh flow theory to analyze the flow field in RDE, and found that the exit flow could be calculated from the conditions downstream and upstream of the detonation wave, and its supersonic velocity. Goto et al. [20] demonstrated that steady performance and heat-load of RDE could be evaluated by the method used in conventional rocket engines.

As already mentioned, typical RDE combustors have an annular channel between the outer and inner cylinders, which are thought to be necessary to sustain detonation waves. However, several recent studies observed that RDEs without an inner cylinder also generate a rotating, continuous detonation wave [21-24]. Tang et al. [21] numerically demonstrated that detonation waves could rotate continuously in a cylindrical RDE combustion chamber. In experiments, Wei et al. [22] and Anand et al. [23] later confirmed the stable realization of rotating detonation waves in a cylindrical RDE combustion chamber, although they did not measure thrust. Kawasaki et al. [24] investigated the

https://doi.org/10.2514/1.J058322
AIAA JOURNAL, Vol. 58, No. 12, pp.5107-5116, December 2020

influence of the inner-cylinder radius on RDE thrust performance, and suggested the critical condition of mass flux. A cylindrical RDE without an inner cylinder has many advantages. It is free from potential severe thermal problems involving the inner cylinder. Removing the inner cylinder can also realize a simpler and more compact structure. Even RDE with quite short and simple combustors could offer high performance because RDE exit flow can be high speed without a convergent-divergent nozzle [19], and detonation combustion is completed in a significantly short distance. Cylindrical RDE have the potential to be a completely different form of rocket engine than that with a convergent-divergent nozzle [25], for example, clustering a compact, nozzleless, cylindrical RDE and obtaining a large thrust.

In this study, a cylindrical RDE with an outer wall diameter of d_o = 20 mm was tested in a low-back-pressure environment, and its thrust performance was evaluated. We introduce a thrust mechanism using a control surface analysis for evaluation, and compare it with the thrust measured by a load cell. Combustion completion is analyzed by a comparison between measured thrust and theoretical thrust obtained by the thrust mechanics principle. Finally, the specific impulses of the experiments are evaluated by the ratio of the measured specific impulses to the specific impulse of the correct expansion.

II. Experimental Setup

Figure 1 presents a scheme of the cylindrical RDE used in the experiments, and Figure 2 contains a photograph of the RDE during combustion. As shown in Fig. 1a, the RDE has no inner cylinder and its combustion chamber is a simple cylinder that is not equipped with a conversion/diversion nozzle. The combustion chamber diameter d_o is 20 mm, and the length L is 70 mm. d_o and L were determined to satisfy the geometric conditions to sustain a continuous, rotating detonation wave such as that proposed by Bykovskii et al. [9]. For example, the center radius of injectors ($r_{inj,ox}$ and $r_{inj,f}$) was determined to satisfy the height condition for the combustible mixture layer h under the Chapman-Jouguet (C-J) detonation wave speed of $D_{C\text{-}J}$. The chamber has pressure measurement ports, and the detonation initiator port included gunpowder. The four pressure-measurement ports are located on the bottom (z = 0 mm, p_c), chamber wall (z = 5, 10, 20, 30, 40, 50, and 65 mm, p_5 to p_{65}), and exit surface of the chamber (p_{es}); p_{es} is measured 10 mm from the chamber wall. All pressure sensors are 1 kHz pressure transducers (KELLER Piezoresistive Pressure Transmitter). The initiator is inserted into the port at z = 10 mm. Ethylene and oxygen were used as propellants injected via the doublet hole injectors shown in Fig. 1b and 1c. The diameters of the injector holes are 0.8 mm for both fuel and oxidizer. There are 24 injector holes. The fuel and oxidizer injectors are arranged in circles with diameters of 9 and 15 mm, respectively. Figure 2b is a photograph of the injector surface. All parts of the RDE were made of stainless

https://doi.org/10.2514/1.J058322
AIAA JOURNAL, Vol. 58, No. 12, pp.5107-5116, December 2020

steel, tightened by bolts and nuts as shown in Figure 2a. The RDE was set on a thrust stand in a vacuum chamber, and the experiments were conducted in a vacuum environment. The thrust stand was pre-loaded, and generated thrust was measured by a load cell. The vacuum chamber had a window for axial visualization. Self-luminescence in the combustor chamber was captured using a high-speed camera set up outside the vacuum chamber. Another camera was placed inside the chamber to take high-spatial-resolution color images of exhaust plumes. Figure 2c shows an image captured by the inside camera.

The mass flow rate was determined and controlled by the orifices downstream of the high-pressure tanks. The following choking equation was used to determine ideal mass flow rate $\dot{m}_{\mathrm{i}}$:

$$\dot{m}_{\mathrm{i}} = \frac{p_{\mathrm{tank}} A_{\mathrm{ori}}}{\sqrt{RT_{\mathrm{p}}}} \sqrt{\gamma \left(\frac{2}{\gamma+1}\right)^{\frac{\gamma+1}{\gamma-1}}} \tag{1}$$

Actual mass flow rate $\dot{m}$ was calculated by

$$\dot{m} = C_d \dot{m}_{\mathrm{i}} \tag{2}$$

where C_{d} is the mass flow coefficient obtained by calibration tests. In the calibration tests, gas is exhausted from injectors without combustion for operational duration t_{ope}, tank mass decrease Δm, and C_{d} is calculated as follows:

$$C_{\mathrm{d}} = \frac{\Delta m}{t_{\mathrm{ope}}} \frac{1}{\dot{m}_{\mathrm{i}}} \tag{3}$$

$\dot{m}_{\mathrm{i}}$ is calculated from Eq. (1). The mass flow rate is regarded as constant within a short duration because the tank volumes (48±1 l) are sufficiently large. The flow was choked at the injector holes before ignition because the pressure of the plenum chambers was controlled to be higher than the critical (choking) pressure. The mass flow rate could also be calculated using the time-averaged plenum pressures before ignition and the geometry of the injector. Equation (4) was used to calculate the mass flow rate from plenum pressure.

$$\dot{m}_{\mathrm{i}} = \frac{p_{\mathrm{ple}} A_{\mathrm{inj}}}{\sqrt{RT_{\mathrm{p}}}} \sqrt{\gamma \left(\frac{2}{\gamma+1}\right)^{\frac{\gamma+1}{\gamma-1}}} \tag{4}$$

Choking of the injectors is assumed here, but the detonation wave propagates on the injector surface and it is possible that local pressure was high downstream of some injector holes. This means that injection could not be choked at some injectors. However, at least averaged mass flow rate was constant via control by the choking orifices upstream of the RDE.

https://doi.org/10.2514/1.J058322
AIAA JOURNAL, Vol. 58, No. 12, pp.5107-5116, December 2020

III. Results and Discussion

Table 1 presents the experimental conditions and a summary of the measurement results. The experiments were conducted under various propellant mass flow rate conditions from 8±1 to 45±1 g/s. We considered the application of the research to be a kick-motor for a spacecraft. Therefore, we operated the RDE under fuel-rich, low-back-pressure conditions. Equivalent ratios were in the range of 1.85±0.33 except in Test 4. The vacuum chamber was evacuated to 6±1 kPa before operation of the RDE except in Tests 1 and 6. We did not conduct experiments in fuel-lean or high-back-pressure conditions, but we consider the effect of the equivalent ratio was probably low because the experimental results of Test 4 (comparatively low equivalent condition) were consistent with other results. The specific impulse ($I_{sp} = \bar{F}_L/\dot{m}g$) was calculated from the averaged load cell thrust ($\bar{F}_L$) and the mass flow rate ($\dot{m}$).

A. Experimental results and internal flow analysis based on pressure distribution

Figure 3 shows the time history of the plenum pressures (Fig. 3a), chamber pressures (Fig. 3b), and thrust measured by the load cell (Fig. 3c). The two regions between vertical dashed lines in Fig. 3 show the time-averaged duration, the cold flow duration (-0.2–0.0 s), and the combustion duration (0.1–0.4 s). The thrust performances listed in Table 1 were averaged in the latter duration. The plenum pressures $p_{ple,\,ox}$ and $p_{ple,\,f}$ were almost steady during both the cold flow and combustion durations. This means injection during combustion duration was choked, because plenum pressure increases in non-choking condition in order to sustain mass flow rate, which is controlled by the upstream orifices. We then used the averaged chamber pressures (p_c and p_5 to p_{65}) and averaged load cell thrust $\bar{F}_L$ of the combustion duration for analysis. In addition, thrust was generated before ignition due to propellant injection. Therefore, we define F_c as the cold flow thrust, which is averaged load cell thrust during the cold flow duration.

Figure 4 shows typical axial photographs of self-luminescence in the combustion chamber. The RDE was operated with a single detonation-like wave in Tests 3–8, whereas the propagation of a detonation-like wave sometimes appeared but was not stable in Test 2, and no wave was observed in Test 1. Tests 1 and 2 were comparatively low mass flow conditions, and the forms of wave propagation were clearly different from other test cases. We considered those waves to be weakly coupled detonation waves [26] caused by insufficient mixing of the propellants, because the wave velocities were comparatively slow. Figure 5 also shows the velocities of the rotating (weakly coupled) detonation waves of Tests 3–8. In order to obtain the velocities of the waves, we had to determine the diameter where the wave was propagating. Strong self-luminescence was observed in the area between d = 10 and 20 mm. We assume

https://doi.org/10.2514/1.J058322
AIAA JOURNAL, Vol. 58, No. 12, pp.5107-5116, December 2020

that diameter of propagation was d = 15 mm (average of d = 10 and 20 mm) in the following discussion. The velocities of the (weakly coupled) detonation waves were then approximately 1200–1350 m/s in Tests 3–8.

The speeds were evaluated as the averaged values within 10 arbitrary revolutions of rotating waves. Upper and lower values of error bars in Fig. 5 represent the wave velocities calculated with d = 20 and 10 mm, respectively. The velocities of the (weakly coupled) detonation waves were approximately 48–53% of each C-J detonation velocity $D_{C\text{-}J}$, and 97–107% of each sound velocity calculated from NASA-CEA with constant-pressure combustion mode by inputting combustion pressure p_c and equivalent ratio Φ [27]. Although wave velocities seem close to sonic velocity, the actual mixture in a RDE combustor should include the unburned gas, and therefore actual sonic velocities must be less than the theoretical velocities obtained from CEA. In addition, some research indicates that a wave velocity can be much slower than the wave speed of C-J detonation [9, 28]. Hence, wave velocities appeared supersonic, and the combustion wave was likely driven by some effect of the detonation combustion process.

Figure 6a shows pressure distributions along the z-direction. Pressure at z = 0 (p_c) was higher if mass flow rate $\dot{m}$ was higher, and thus all test cases lined up from Test 1 to Test 8 from bottom to top. The most important case was Test 6 (blue circles), in which the pressure distribution was the most detailed. The distribution trend was similar to that measured by Rankin et al. [29]. The slope of the distribution was different between the upstream ($z \leq 20$ mm) and downstream ($z \geq 20$ mm). Pressure rapidly decreased near the bottom, and slowly decreased after z = 20 mm. The measured pressure of Test 5 (purple cross) showed the same trend because the pressure measured at z = 30 mm deviated from the extrapolation of pressures near z = 0 mm (purple dashed line).

The distributions also suggest that pressure ratios of exit pressure (p_{65}) to combustion pressure (p_c) were approximately 0.5 in all test cases except Test 1. The ratio 0.5 is close to the ratio of critical pressure p^* to bottom pressure p_o of isentropic flow calculated from the following equation:

$$\frac{p^*}{p_o} = \left(\frac{2}{\gamma+1}\right)^{\frac{\gamma}{1-\gamma}} \tag{5}$$

and Rayleigh flow

$$\frac{p_o}{p^*} = \frac{1+\gamma}{1+\gamma M^2} \tag{6}$$

when we assume the inlet Mach number M_i is 0.1–0.3 (in the Rayleigh assumption), and γ is 1.1–1.2 (in both assumptions). The results suggest that internal flow near the combustor exit should reach sonic velocity. Figure 6b shows the Mach number distribution calculated from the Rayleigh flow theory. We calculated by Rayleigh flow

https://doi.org/10.2514/1.J058322
AIAA JOURNAL, Vol. 58, No. 12, pp.5107-5116, December 2020

because we consider that heat release is a major factor of flow acceleration. Figure 6b clearly shows that the burned gas may be accelerated to the sonic velocity. The error bars in Fig. 6b indicate the uncertainty of γ and M_i in the calculations. The results also suggest that acceleration is insufficient in Test 1 because the Mach number of $z = 65$ mm was approximately 0.85 only in that test. Test 1 was the case in which no detonation wave was observed. Therefore, the acceleration of the burned gas may be affected by the combustion condition.

We obtained Mach numbers as in Fig. 6b, but the internal flow in the combustor was not a simple isentropic flow or Rayleigh flow even if the flow field could be regarded as a quasi-1-D flow as in previous research [19, 20]. In order to analyze the internal flow of the cylindrical RDE, we assumed that the flow field was affected by growth of a boundary layer (isentropic effect), and heating of a chemical reaction (Rayleigh effect). Figure 7 shows the scheme of the proposed internal flow. We considered that the internal flow was quasi-1-D, and obtained input parameters under two combustion assumptions: constant-pressure combustion (cp assumption); and constant-volume combustion (cv assumption). In the proposed internal flow field, propellant is burned from the bottom (left) to $z = z_{rc.}$ (red dashed line). The propellant releases heat by chemical reaction, and rapidly accelerates by the heat; however, we also assumed that the chemical composition was frozen in order to simplify the problem. Total chemical energy per unit mass released by the reaction is defined as Q. A boundary layer also developed from the bottom to the exit, and acceleration by the effect of convergent flow was caused throughout the flow field. Orange and blue lines indicate concepts of Mach number and pressure profile, respectively. Propellant acceleration satisfied the conservation laws of continuity, motion, and energy for steady 1-D flow as follows [30]:

$$\frac{1}{\rho}\frac{d\rho}{dz} + \frac{1}{u}\frac{du}{dz} + \frac{1}{A_{ef}}\frac{dA_{ef}}{dz} = 0 \tag{7}$$

$$u\frac{\mathrm{du}}{\mathrm{dz}} + \frac{1}{\rho}\frac{dp}{dz} = 0 \tag{8}$$

$$\frac{\mathrm{d}}{\mathrm{dz}}\left[\rho u A_{ef}\left(\frac{\gamma}{\gamma-1}\frac{p}{\rho} + \frac{u^2}{2} - \lambda Q\right)\right] = 0 \tag{9}$$

where A_{ef} is an efficient cross-sectional area of the chamber reduced by the boundary layer, and λ $(0 \le \lambda \le 1)$ is the reaction progress variable. A_{ef} is obtained by the following equation:

$$A_{ef} = \frac{\pi}{4}(d_O - 2\delta^*)^2 \tag{10}$$

where δ^* is the displacement thickness of the boundary layer theory. From the boundary layer theory of turbulent flow [31], it is known that δ^*/z is a function of $R_z^{1/5}$ ($R_z = uz/\nu$: Reynolds number) as follows:

https://doi.org/10.2514/1.J058322
AIAA JOURNAL, Vol. 58, No. 12, pp.5107-5116, December 2020

$$\frac{\delta^*}{z} = \frac{k}{R_z^{-1/5}} \tag{11}$$

where k is a constant coefficient. For instance, k is 0.046 on a flat plate flow [31]. The reaction progress variable λ is $\lambda = 0$ at $z = 0$, and $\lambda = 1$ at $z \geq z_{\mathrm{rc}}$, which means chemical reaction is completed at $z = z_{\mathrm{rc}}$. We assume that the chemical reaction progressed rapidly near $z = 0$ and was gradually completed near $z = z_{\mathrm{rc}}$. In order to satisfy the assumption, λ is defined as follows:

$$\begin{cases} \lambda = -\frac{1}{z_{\mathrm{rc}}} z(z - 2z_{\mathrm{rc}}) & (z \leq z_{\mathrm{rc}}) \\ \lambda = 1 & (z > z_{\mathrm{rc}}) \end{cases} \tag{12}$$

Examples of transitions of δ^* and λ in the chamber are shown in Fig. 8.

We solve Eq. (7) – (9) numerically using the Euler method. We assume parameters γ, R, ν are constant, and as mentioned above, and obtain the parameters under the cp and cv assumptions. These are obtained by the NASA-CEA constant-pressure combustion mode, inputting p_{c} and Φ, and constant-volume combustion mode, inputting ρ and Φ. Input ρ is calculated from p_{c} and the combustion temperature, and obtained by iterations. The other parameters were measured in experiments. Total released chemical energy per unit mass Q was calculated by the chemical composition after combustion, which was also obtained by NASA-CEA. Initial pressure p_{c} was the combustor pressure, and initial Mach number M_{i} was obtained as follows:

$$M_{\mathrm{i}} = \frac{\overline{u_{\mathrm{inj}}}}{a_{\mathrm{unburned}}} = \frac{\dot{m}/\rho A_c}{(\sqrt{\gamma RT})_{\mathrm{unburned}}} \tag{13}$$

where A_{c} is a cross-sectional area of the chamber. $\overline{u_{\mathrm{inj}}}$ is the spatial-averaged velocity of the injection as if the propellant of mass flow rate $\dot{m}$ were injected through the whole area of A_{c}.

The calculation results are shown in Fig. 8a and 8b. The transitions were calculated under the same conditions as Test 6 (p_{c} = 252 kPa and Φ = 1.8). γ was 1.14, R was 438.8 J/kg·K, and ν was 0.000629 m^2/s in the cp combustion assumption; meanwhile, γ was 1.14, R was 454.7 J/kg·K, and ν was 0.000664 m^2/s in the cv combustion assumption. z_{rc} was determined to be 20 mm, since the slope of the pressure transition of Test 6 changed at z = 20 mm. k is an unknown parameter and here we set k as 0.17 in the cp assumption and 0.48 in the cv assumption so that the theoretical flow reached sonic velocity.

The theoretical pressure transition of the cp assumption was close to the experimental transition of Test 6 in the upstream region. On the other hand, the theoretical pressure in the downstream region showed a trend similar to the experimental, but was slightly higher. The difference may have been caused by factors not considered here, such as

https://doi.org/10.2514/1.J058322
AIAA JOURNAL, Vol. 58, No. 12, pp.5107-5116, December 2020

2- (or 3-) D flow effect. Theoretical Mach number was very close to sonic velocity, but also slightly lower than 1. At least the trends of the theoretical and experimental transitions were very close in the cp combustion assumption. In contrast, the theoretical pressure calculated by the cv assumption was different from the experimental. This may mean that time-averaged or low-frequency phenomenon inside the RDE can be explained using cp combustion. We conclude that the structure of the internal flow of the cylindrical RDE could be explained to some extent by the proposed structure with the cp combustion assumption.

B. Thrust estimation from pressure and momentum exchange using control surface theory

Next, we analyze the completion of RDE combustion by thrust and pressure measurements. First, we show how the time-averaged thrust of the RDE was estimated by the time-averaged pressure loaded on a control surface and the momentum exchange through the surface. Figure 9 shows a control surface (control surface 1) set on the RDE surface including the injector plate. The total forces loaded on a control surface are expressed as [16]:

$$\boldsymbol{F} = \int_A \rho \boldsymbol{v}\boldsymbol{v} \cdot \boldsymbol{n}\, \mathrm{d}S + \int_A p\boldsymbol{n}\, \mathrm{d}S \tag{14}$$

The viscosity of gases, friction, and body forces are neglected here. The first term on the right side of Eq. (14) is derived from the momentum exchange between the inside and outside of the control volume, and the second term is derived from the pressure on the control surface. Focusing on the axial force, we introduce simplified axial force F_{T} defined as follows:

$$F_{\mathrm{T}} = \dot{m} v_{\mathrm{p}} + (p_c - p_b) A_c \tag{15}$$

As shown in Fig. 9, propellant was supplied through the control surface, and its injection into the combustion chamber was regarded as a momentum exchange. The propellants were supplied from gas lines outside of the RDE to the RDE plenums, and they did not contribute to the axis force since they were supplied perpendicular to the axial direction. Therefore, the first term on the right side of Eq. (14) is derived only from the momentum exchange of propellants through the injectors ($\dot{m} v_{\mathrm{p}}$). Moreover, considering only axial forces, pressure is balanced except for that on the injector surface and exit surface. However, while it is possible that the exhaust plume increased pressure at the exit surface and thus axial force, we neglect the effect of the plume. This is because we estimated pressure on the exit surface based on the Prandtl-Meyer flow theory [31], and the estimated pressure was less than 1% of the combustion pressure p_{c}. Moreover, measured pressure on the exit surface (p_{es}) in Table 1 was almost the same as back pressure p_{b}, and Sun et al. [32] also suggested that pressure derived from plumes was less than 1% of main thrust of an RDE in a

https://doi.org/10.2514/1.J058322
AIAA JOURNAL, Vol. 58, No. 12, pp.5107-5116, December 2020

low-back-pressure condition. Hence, the second term in Eq. (14) is expressed as the pressure difference between p_c and back pressure p_b, and the chamber's cross-sectional area A_c is the only place where the pressures are unbalanced.

The variables in Eq. (15), especially for p_c, are time-variant and nonuniform due to the rotating detonation wave. It is difficult to measure such high-frequency fluctuating and nonuniform data. Thus, we considered using time-averaged measurements, and attempted to evaluate the thrust performance of the RDE. The momentum thrust, however, could not be obtained as $\dot{m}v_p$ since propellant injection velocity v_p was unknown. Therefore, we used cold flow thrust F_c instead of $\dot{m}v_p$, because thrust during the cold flow duration was derived only from the propellant injection from the plenums to the combustor; F_c was then regarded as thrust derived from momentum exchange through the injector surface. We assume here that the velocity of injection v_p was constant before ignition and during RDE operation. This is because the plenum pressure was constant during operation in all cases, meaning injection was constantly choked in the RDE.

Figure 10 compares $\bar{F}_L$ (blue squares), F_T (red circles), the pressure thrust of F_T (=$\dot{m}v_p$, purple circles), and momentum thrust of F_T (=$(p_c - p_b)A_c$, orange squares) for all cases. Momentum thrust and pressure thrust of F_T are the first and second terms of Eq. (15), respectively. F_T almost agreed with $\bar{F}_L$ in all cases, though F_T was a bit small in Test 8 because some experimental measurement problems may have resulted in the underestimation of $\dot{m}v_p$ (= F_c). This result suggests that we can evaluate the measured thrust by the thrust calculated from momentum and pressure measurement based on the control surface theory.

We indicate that the combustion was perfectly completed inside the RDE chamber by ensuring that the measured thrust was close to the theoretical thrust using the thrust evaluation method mentioned above. We showed that a measured thrust agreed with a thrust calculated based on momentum exchange and pressure measurement for a certain control surface. The method is applicable if the control surface is changed [16], and we then set another control surface. Figure 11 shows the scheme of control surface 2, set so as to cover the RDE, and the area of pressure loading and momentum exchange at the chamber exit. Estimated axial thrust F_S of control surface 2 is then expressed as:

$$F_S = \dot{m}v_e + (p_{65} - p_b)A_c \tag{16}$$

In Eq. (16), v_e is the velocity of the gas at the chamber exit and p_{65} is regarded as the pressure there. Whereas p_{65} was measured, v_e is unknown. Therefore, we assume that v_e is sonic velocity as suggested by the previous section, and thus obtain v_e from NASA-CEA with a cp combustion mode. We input $p_{c,th}$ as a theoretical combustion pressure, $p_{c,th}/p_b$ as

https://doi.org/10.2514/1.J058322
AIAA JOURNAL, Vol. 58, No. 12, pp.5107-5116, December 2020

the pressure ratio, and Φ as the equivalent ratio. Here, we obtain p_c from following equation proposed by Goto, et al. [20]:

$$p = \frac{c^*}{A_t}\dot{m} \tag{17}$$

c^* is the characteristic exhaust speed, and A_t is a cross-sectional area of the throat. To obtain theoretical p_c, we assume that c^* = 1800 m/s, because the ideal c^* of ethylene-oxygen propellant is around 1800 m/s, and the c^* efficiency of RDE is close to 1 [20]. A_t is regarded as a cross-sectional area of the combustor in this RDE. Then, v_e was calculated as a theoretical sonic velocity, or the theoretical velocity at a throat. In addition, theoretical thrust $F_{S,\,theory}$ on the assumption that the exhaust velocity is sonic velocity is defined as:

$$F_{S,theory} = \dot{m}v_{e,theory} + \left(p_{e,theory} - p_b\right)A_c \tag{18}$$

$p_{e,\,theory}$ is calculated from CEA under the same conditions used to calculate v_e.

Figure 12 presents a comparison between $\bar{F}_L$ (blue squares) and $F_{S,\,theory}$ (black line). The pressure thrust of $F_{S,\,theory}$ (=$\dot{m}v_{e,theory}$, purple line), and momentum thrust of $F_{S,\,theory}$ (=$\left(p_{e,theory} - p_b\right)A_c$, orange line) are also plotted. Errors in $\bar{F}_L$ are within 10% except for Test 1. The $\bar{F}_L$ of Test 1, where detonation-like waves were not observed, was approximately 75% of $F_{S,\,theory}$. This means the measured thrusts were in good agreement with theoretical thrusts at each combustion pressure, and suggests that RDE combustion was perfectly completed inside the chamber.

Finally, Figure 13 is a comparison of $\bar{F}_L$, F_T, and $F_{S,\,theory}$. Thrusts are nondimensionalized by $F_{S,\,theory}$. $\bar{F}_L$ (blue squares) corresponds with F_T (red circles) in all test cases. Again, F_T should agree with $\bar{F}_L$, since they are the measured thrusts from two points of view, and the result verifies this assumption. $\bar{F}_L$ and F_T also agree with $F_{S,\,theory}$ except for Test 1. These findings indicate again that RDE thrust was estimated from pressure and momentum exchange considering the control surface, and that RDE combustion was completed in the chamber. The Test 1 results also suggest that thrust performance decreases compared to the theoretical performance if the detonation-like wave does not appear.

C. Thrust performance of a cylindrical RDE by means of I_{sp} evaluation

Figure 14 contains plots of specific impulses (closed circles). The horizontal axis is the nondimensional pressure p_c/p_b. $I_{sp,\,fully\ correct\ expanded\ theory}$ and $I_{sp,\,FS\ theory}$ are also shown in the figure. $I_{sp,\,fully\ correct\ expanded\ theory}$ is I_{sp} when gas with pressure p_c is expanded to p_b, and $I_{sp,\,FS\ theory}$ is I_{sp} calculated from $F_{S,\,theory}$ ($I_{sp,\,FS\ theory} = F_S/\dot{m}g$). These theoretical I_{sp} were calculated by NASA-CEA. The specific impulses of the cylindrical RDE were more than 80% of $I_{sp,\,fully\ correct}$

https://doi.org/10.2514/1.J058322
AIAA JOURNAL, Vol. 58, No. 12, pp.5107-5116, December 2020

$_{\text{expanded theory}}$, whereas the I_{sp} of another cylindrical RDE examined by Kawasaki et al. [24] was less than 80%, and this performance was close to an annular RDE observed in previous research. This suggests that with proper conditions (such as the ratio of injector area to chamber area, or the arrangement of injectors), a cylindrical RDE exhibits thrust performance equal to that of an annular RDE. In addition, it is implied that RDE thrust performance increases if the RDE has a divergent nozzle. From the fully expanded theory, performance will increase by 20%. While the RDE with a divergent nozzle increases thrust performance, nozzleless and cylindrical RDE has high thrust performance with a simple structure.

IV. Conclusions

We tested a cylindrical nozzleless RDE in a low-back-pressure environment with variations in the propellant mass flow rate from 8–45 g/s. Under conditions of 22 g/s or higher, a single self-luminescence region rotating in the combustor chamber was observed by axial-visualization and was assumed to be a rotating detonation wave. When the mass flow rate was 15 g/s, the propagation of a rotating detonation wave was not maintained continuously, and no rotating region appeared under the condition of 8 g/s. We measured the pressure distributions and proposed the structure of the internal flow of the cylindrical RDE based on these measures. Heat release by chemical reaction and conversion by boundary layer development were the factors affecting flow acceleration in the proposed internal flow structure. Theoretical pressure distribution was calculated numerically, and was close to experimental pressure distribution. Results suggested that burned gas should reach sonic velocity at the chamber exit. Moreover, RDE thrust was estimated using pressure and momentum exchange through a control surface, and was confirmed because the load cell thrust $\bar{F}_{\mathrm{L}}$ agreed with the estimated thrust on control surface 1, which is F_{T}. $F_{\mathrm{S,\,theory}}$ was defined as the estimated thrust on the assumption that the exit plume is sonic flow, and $\bar{F}_{\mathrm{L}}$ agreed with F_{T}, and $F_{\mathrm{S,\,theory}}$. This suggests that the measured thrust of the RDE was close to the certain theoretical thrust, and RDE combustion was perfectly completed inside the chamber. Additionally, the specific impulses of the cylindrical RDE were more than 80% of the specific impulse of fully correct expanded flow. This was almost the same as an annular RDE value observed in previous research. The chamber designs, such as the outer wall radius, arrangement of the injector, and ratio of injector area to combustion chamber area may affect thrust performance. It is also expected that the performance of the cylindrical RDE will increase by approximately 20% based on the fully correct expansion theory.

https://doi.org/10.2514/1.J058322
AIAA JOURNAL, Vol. 58, No. 12, pp.5107-5116, December 2020

Acknowledgments

This study was financially supported by JSPS KAKENHI Grant Numbers JP19H05464, JP18KK0127, JP17H03480, JP17K18937, and by the Institute of Space and Astronautical Science of the Japan Aerospace Exploration Agency.

References

[1] Fickett, W., and Davis, W. C., *Detonation: Theory and Experiment*, Dover Publications, New York, 2000.
doi: 10.1017/S0022112001265604

[2] Lee, J. H. S., *The Detonation Phenomenon*, Cambridge University Press, Cambridge, 2008.
doi: 10.1017/CBO9780511754708

[3] Law, C. K., *Combustion Physics*, Cambridge University Press, Cambridge, 2006.
doi: 10.1017/CBO9780511754517

[4] Wolanski, P., "Detonative Propulsion," *Proceedings of the Combustion Institute*, Vol. 34, No.1, 2013, pp. 125-158.
doi: 10.1016/j.proci.2012.10.005

[5] Kailasanath, K., "Review of Propulsive Applications of Detonation Waves," *AIAA Journal*, Vol. 38, No. 9, 2000, pp. 1698–1708.
doi: 10.2514/2.1156

[6] Lu, F. K., and Braun, E. M., "Rotating Detonation Wave Propulsion: Experimental Challenges, Modeling, and Engine Concepts," *Journal of Propulsion and Power*, Vol. 30, No. 5, 2014, pp. 1125-1142.
doi: 10.2514/1.B34802

[7] Li, J. M., Teo, C. J., Khoo, B. C., Yao, S., and Wang, C., (eds.), *Detonation Control for Propulsion Pulse Detonation and Rotating Detonation Engines*, Springer, Cham, Switzerland, 2018.
doi: 10.1007/978-3-319-68906-7

[8] Roy, G. D., Frolov, S. M., Borisov, A. A., Netzer, D. W., "Pulse Detonation Propulsion: Challenges, Current Status, and Future Perspective," *Progress in Energy and Combustion Science*, Vol. 30, No. 6, 2004, pp. 545-672.
doi: 10.1016/j.pecs.2004.05.001

[9] Bykovskii, F. A., Zhdan, S. A., and Vedemikov, E. F., "Continuous Spin Detonations," *Journal of Propulsion and Power*, Vol. 22, No. 6, 2006, pp. 1204–1216.
doi: 10.2514/1.17656

https://doi.org/10.2514/1.J058322
AIAA JOURNAL, Vol. 58, No. 12, pp.5107-5116, December 2020

[10] George, A. S., Driscoll, R., Anand, V., and Gutmark, E., "On the Existence and Multiplicity of Rotating Detonations," *Proceedings of the Combustion Institute*, Vol. 36, No. 2, 2017, pp. 2691–2698.
doi: 10.1016/j.proci.2016.06.132

[11] Nakayama, H., Moriya, T., Kasahara, J., Matsuo, A., Sasamoto, Y., and Funaki, I., "Stable Detonation Wave Propagation in Rectangular-Cross-Section Curved Channels," *Combustion and Flame*, Vol. 159, No. 2, 2012, pp. 859–869.
doi: 10.1016/j.combustflame.2011.07.022

[12] E. Wintenberger, J. M. Austin, M. Cooper, S. Jackson, and J. E. Shepherd. "Analytical Model for the Impulse of Single-Cycle Pulse Detonation Tube", *Journal of Propulsion and Power*, Vol. 19, No. 1, 2003, pp. 22-38.
doi: 10.2514/2.6099

[13] Endo, T., Kasahara, J., Matsuo, A., Sato, S., Inaba, K., and Fujiwara, T., "Pressure History at the Thrust Wall of a Simplified Pulse Detonation Engine," *AIAA Journal*, Vol. 42, No. 9, 2004, pp. 1921-1930.
doi: 10.2514/1.976

[14] Rankin, B. A., Fotia, M. L., Naples, A. G., Stevens, C. A., Hoke, J. L., Kaemming, T. A., Theuerkauf, S. W., and Schauer, F. R., "Overview of Performance, Application, and Analysis of Rotating Detonation Engine Technologies," *Journal of Propulsion and Power*, Vol. 33, No. 1, 2017, pp. 131-143.
doi: 10.2514/1.B36303

[15] Fotia, M. L., Hoke, J. L., and Schauer, F. R., "Experimental Performance Scaling of Rotating Detonation Engines Operated on Gaseous Fuels," *Journal of Propulsion and Power*, Vol. 33, No. 5, 2017, pp. 1187-1196.
doi: 10.2514/1.B36213

[16] Shepherd, J. E., and Kasahara, J., "Analytical Models for the Thrust of a Rotating Detonation Engine," CaltechGALCITFM, California Institute of Technology, Pasadena, CA, 2017 (unpublished).

[17] Fievisohn, R. T., and Yu, K. H., "Steady-State Analysis of Rotating Detonation Engine Flowfields with the Method of Characteristics," *Journal of Propulsion and Power*, Vol. 33, No. 1, 2017, pp. 89-99.
doi:10.2514/1.B36103

[18] Mizener, A. R., and Lu, F. K., "Low-Order Parametric Analysis of a Rotating Detonation Engine in Rocket Mode," *Journal of Propulsion and Power*, Vol. 33, No. 6, 2017, pp. 1543-1554.
doi:10.2514/1.B36432

[19] Knowlen, C., Wheeler, E. A., and Kurosaka. M., "Thrusting Pressure and Supersonic Exhaust Velocity in a Rotating Detonation Engine," *2018 AIAA Aerospace Sciences Meeting,* AIAA Paper 2018-1884, Kissimmee, FL, 2018.
doi: 10.2514/6.2018-0884

https://doi.org/10.2514/1.J058322
AIAA JOURNAL, Vol. 58, No. 12, pp.5107-5116, December 2020

[20] Goto, K., Nishimura, J., Kawasaki, A., Matsuoka, K., Kasahara, J., Matsuo, A., Funaki, I., Nakata, D., Uchiumi, M., and Higashino, K., "Propulsive Performance and Heating Environment of Rotating Detonation Engine with Various Nozzles," *Journal of Propulsion and Power*, Vol. 35, No. 1, 2019, pp. 213-223.
doi: 10.2514/1.B37196

[21] Tang, X. M., Wang, J. P., and Shao, Y. T. "Three-Dimensional Numerical Investigations of the Rotating Detonation Engine with a Hollow Combustor," *Combustion and Flame*, Vol. 162, No. 4, 2015, pp. 997-1008.
doi: 10.1016/j.combustflame.2014.09.023

[22] Lin, W., Zhou, J., Liu, S., and Lin, Z. "An Experimental Study on CH4/O2 Continuously Rotating Detonation Wave in a Hollow Combustion Chamber," *Experimental Thermal and Fluid Science*, Vol. 62, 2015, pp. 122-130.
doi: 10.1016/j.expthermflusci.2014.11.017

[23] Anand, V., St. George, A. C., and Gutmark, E. J. "Hollow Rotating Detonation Combustor," *54th AIAA Aerospace Sciences Meeting*, AIAA Paper 2016-0124, San Diego, CA, 2016.
doi: 10.2514/6.2016-0124

[24] Kawasaki, A., Inakawa, T., Kasahara, J., Goto, K., Matsuoka, K., Matsuo, A., and Funaki, I "Critical Condition of Inner Cylinder Radius for Sustaining Rotating Detonation Waves in Rotating Detonation Engine Thruster," *Proceedings of the Combustion Institute*, Vol. 37, No. 3, 2019, pp. 3461-3469.
doi: 10.1016/j.proci.2018.07.070

[25] Sutton, G. P., and Biblarz, O., *Rocket propulsion elements*, 9th ed., John Wiley & Sons Inc., New York, 2016.

[26] Jason, R. B., and Kenneth, H. Y., "Mixing in Linear Detonation Channel with Discrete Injectors and Side Relief," *AIAA Scitech 2019 Forum*, San Diego, CA, AIAA paper 2019-1014, Jan 2019.
doi: 10.2514/6.2019-1014

[27] Gordon, S., and McBride, B. J., "Computer Program for Calculation of Complex Chemical Equilibrium Compositions and Applications," NASA RP-1311, 1996.

[28] Wilhite, J., Driscoll, R., St George, A., Anand, V., and Gutmark, E., "Investigation of a Rotating Detonation Engine Using Ethylene-Air Mixtures," *Proceedings of the 54th AIAA Aerospace Sciences Meeting*, San Diego, CA, AIAA Paper 2016-1650, Jan 2016.
doi:10.2514/6.2016-1650

[29] Rankin, B. A., Richardson, D. R., Caswell, A. W., Naples, A. G., and Hoke, J. L., "Chemiluminescence Imaging of an Optically Accessible Non-Premixed Rotating Detonation Engine," *Combustion and Flame*, Vol. 176, No. 1, 2017, pp. 12–22.
doi: 10.1016/j.combustflame.2016.09.020

[30] Lee, J. H. S., *The Detonation Phenomenon*, Cambridge Univ. Press, New York, 2008.

https://doi.org/10.2514/1.J058322
AIAA JOURNAL, Vol. 58, No. 12, pp.5107-5116, December 2020

doi: 10.1017/CBO9780511754708

[31] Spurk, J. H., and Aksel, N., *Fluid mechanics*, 2nd ed., Springer, Berlin, 2008.

doi: 10.1007/978-3-540-73537-3

[32] Sun, J., Zhou, J., Liu, S., Lin, Z., and Lin, W. "Plume Flowfield and Propulsive Performance Analysis of a Rotating Detonation Engine," *Aerospace Science and Technology*, Vol. 81, 2018, pp. 383-393.

https://doi.org/10.2514/1.J058322
AIAA JOURNAL, Vol. 58, No. 12, pp.5107-5116, December 2020

Table 1 Experimental conditions and summary of results

Test	$\dot{m}$ [g/s]	Φ [-]	p_b [kPa]	D (of d = 15 mm) [m/s]	p_c [kPa]	p_{es} [kPa]	F [N]	I_{sp} [s]
1	8±1	1.98±0.03	17±1	-	42±1	15±1	9±7	115±81
2	15±1	1.83±0.02	6±1	-	91±5	10±1	30±6	206±39
3	22±1	1.69±0.02	6±1	1209±30	144±2	9±1	51±6	238±27
4	27±1	1.29±0.01	6±1	1276±30	173±2	9±1	60±6	226±22
5	33±1	1.67±0.02	6±1	1318±30	230±2	-	78±7	241±23
6	36±1	1.81±0.01	11±2	1328±30	252±3	12±1	88±11	246±31
7	40±1	2.01±0.03	6±1	1329±30	268±2	12±1	97±8	250±21
8	45±1	1.95±0.07	6±1	1333±30	296±6	-	108±7	242±16

https://doi.org/10.2514/1.J058322
AIAA JOURNAL, Vol. 58, No. 12, pp.5107-5116, December 2020

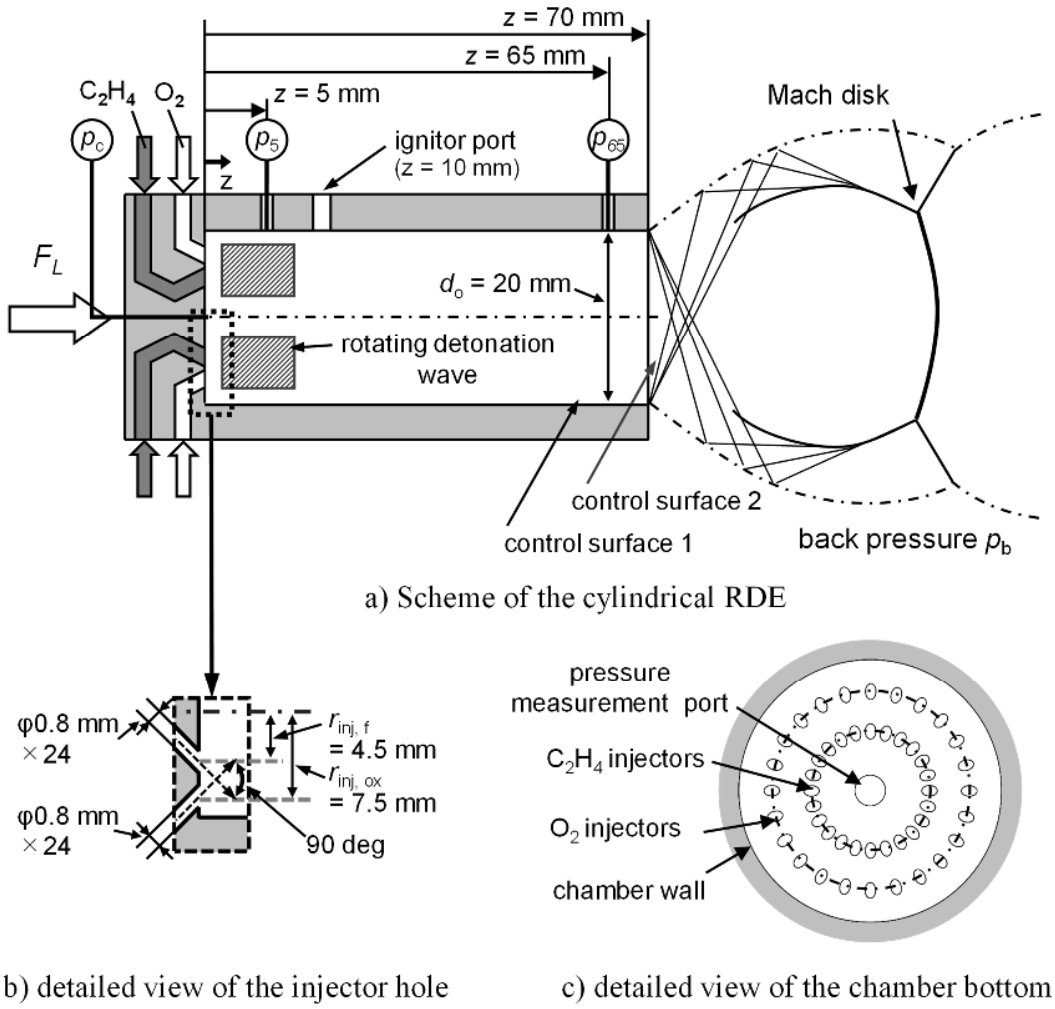

Fig. 1 Schemes of cylindrical RDE: (a) vertical cross-sectional view of a cylindrical RDE including control surface, axial forces loaded on the RDE, and plume of burned gas; (b) detailed view of the injector holes; and (c) detailed view of the chamber bottom from the axial direction.

https://doi.org/10.2514/1.J058322
AIAA JOURNAL, Vol. 58, No. 12, pp.5107-5116, December 2020

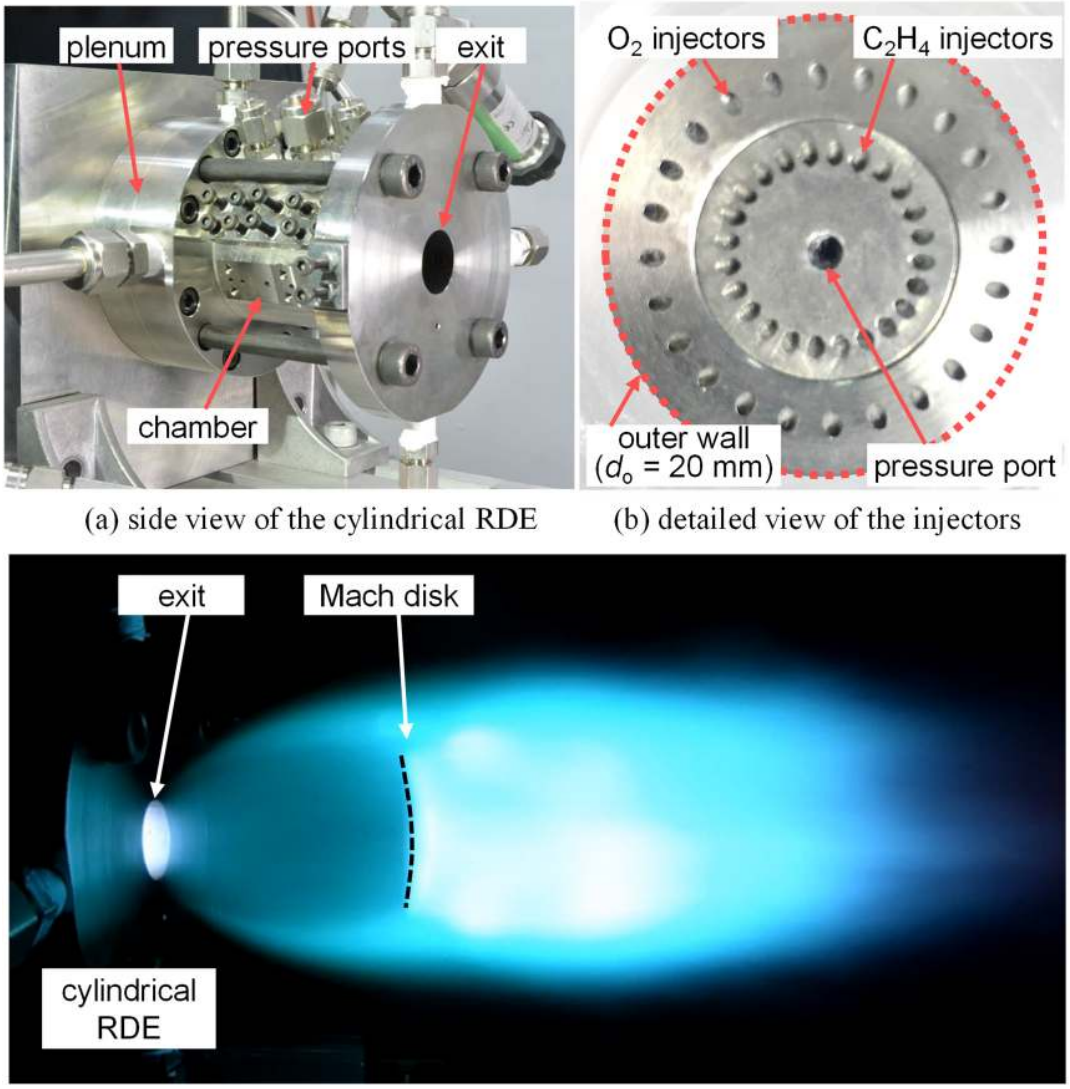

(a) side view of the cylindrical RDE (b) detailed view of the injectors

(c)The RDE and exhaust plume during operation

Fig. 2 RDE photographs: (a) overview of the RDE; (b) detailed view of the injectors; and (c) cylindrical RDE during operation in a vacuum chamber.

https://doi.org/10.2514/1.J058322
AIAA JOURNAL, Vol. 58, No. 12, pp.5107-5116, December 2020

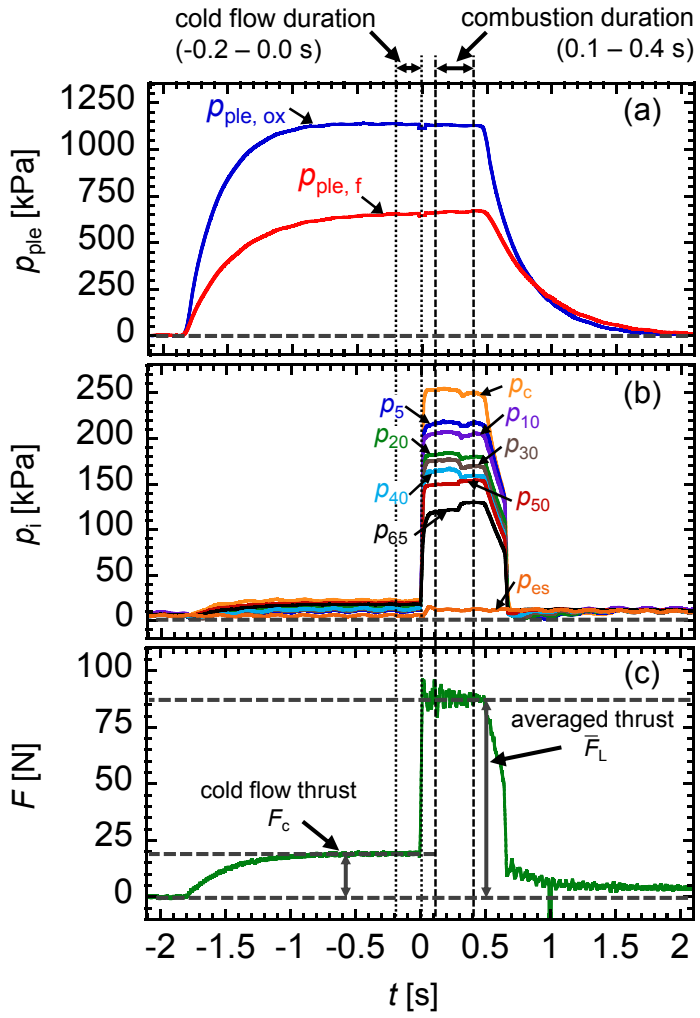

Fig. 3 Time histories of: (a) plenum pressures ($p_{ple, ox}$, $p_{ple, f}$); (b) chamber pressures (p_c, p_5, p_{65}); and (c) load cell thrust (F) of Test 6. Pressures and thrust are averaged from -0.2 s to 0.0 s as cold flow duration, and from 0.1 s to 0.4 s as combustion duration. Thrust averaged in cold flow duration is regarded as cold flow thrust F_c.

https://doi.org/10.2514/1.J058322
AIAA JOURNAL, Vol. 58, No. 12, pp.5107-5116, December 2020

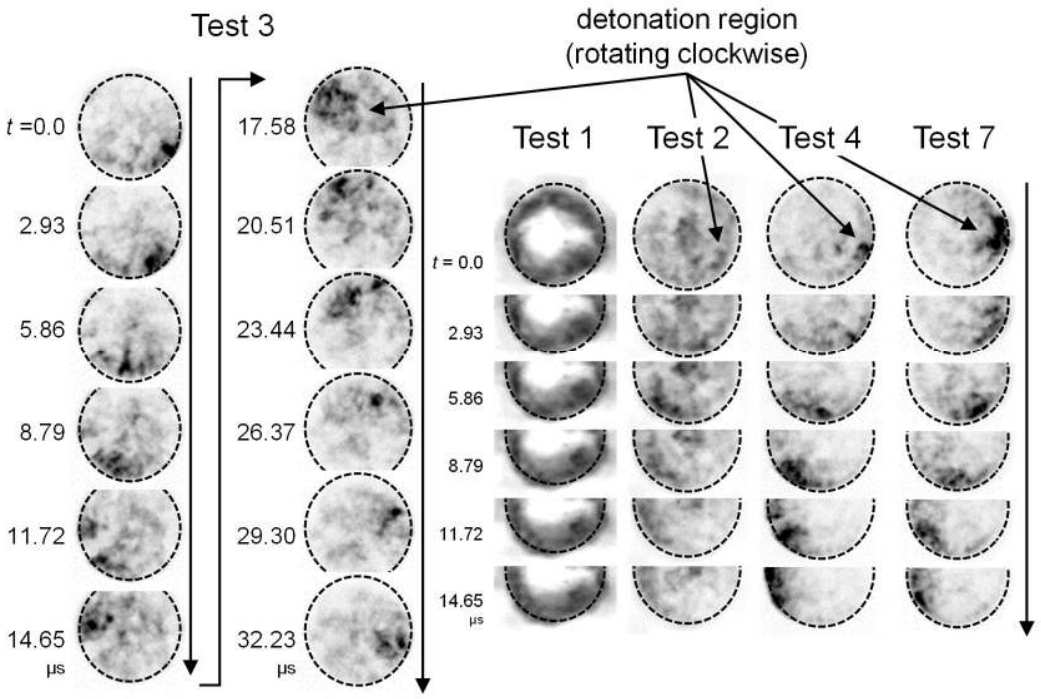

Fig. 4 Typical axial images of rotating detonation wave in a cylindrical RDE from Tests 1–4, and 7. Black and white are reversed in the photographs, and the waves are rotating clockwise.

https://doi.org/10.2514/1.J058322
AIAA JOURNAL, Vol. 58, No. 12, pp.5107-5116, December 2020

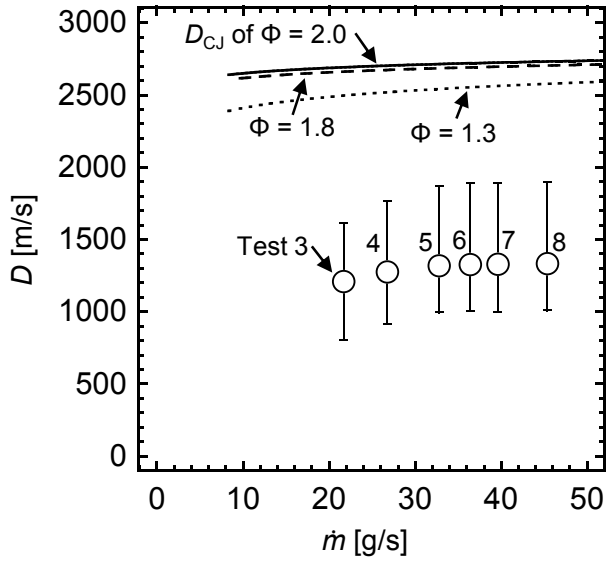

Fig. 5 Velocities of the rotating detonation waves of the cylindrical RDE from Tests 3–8. Lines in the upper part of the graph are wave velocities of the C-J detonation. Circle plots of experimental values are average wave velocities calculated where *d* is 15 mm, and upper/lower errors are wave velocities where *d* is 20/10 mm respectively.

https://doi.org/10.2514/1.J058322
AIAA JOURNAL, Vol. 58, No. 12, pp.5107-5116, December 2020

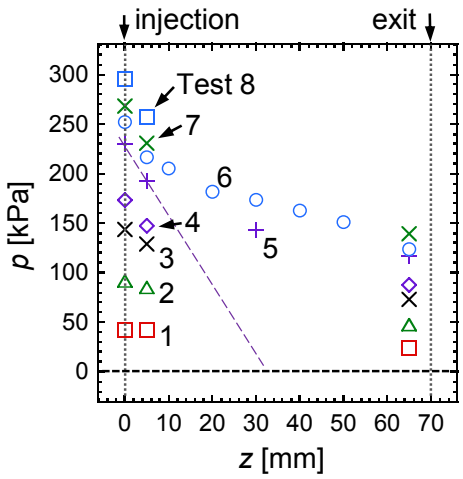

(a) pressure distributions along z-direction

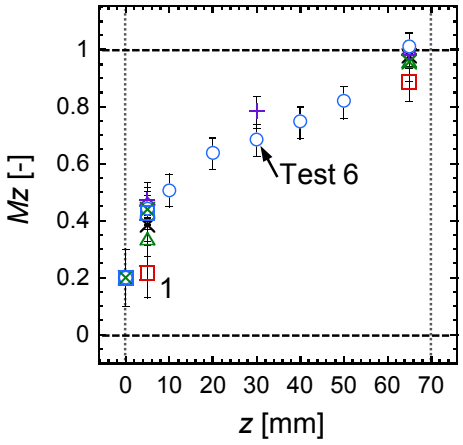

(b) Mach number distributions based on the Rayleigh flow theory.

Fig. 6 (a) Pressure distributions, and (b) Mach number distributions of all test cases along the z-direction. Mach number distributions were calculated based on the Rayleigh flow theory.

https://doi.org/10.2514/1.J058322
AIAA JOURNAL, Vol. 58, No. 12, pp.5107-5116, December 2020

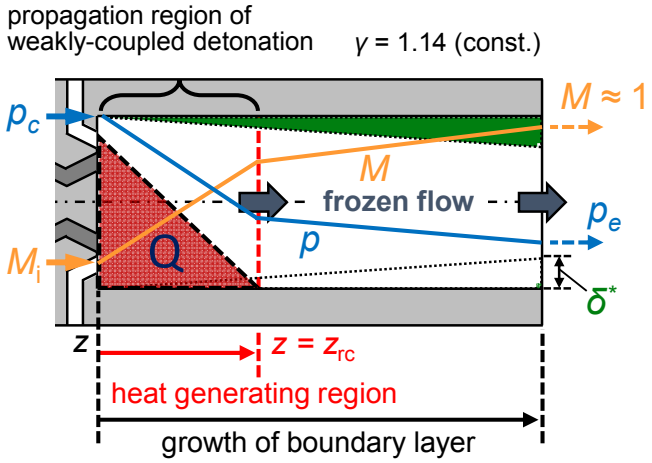

Fig. 7 Scheme of proposed internal flow field. Heat-generating region where a detonation-like wave rotates is ended at $z = z_{h.e.}$, and burned gas is rapidly accelerated in the region. The gas is accelerated further downstream of the heat generating region because the boundary layer grows and flow field is convergent.

https://doi.org/10.2514/1.J058322
AIAA JOURNAL, Vol. 58, No. 12, pp.5107-5116, December 2020

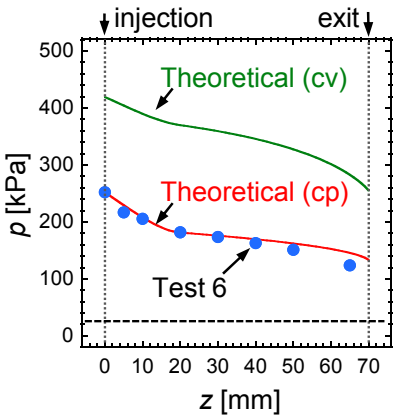

(a) transitions of theoretical pressure and experimental pressure of Test 6

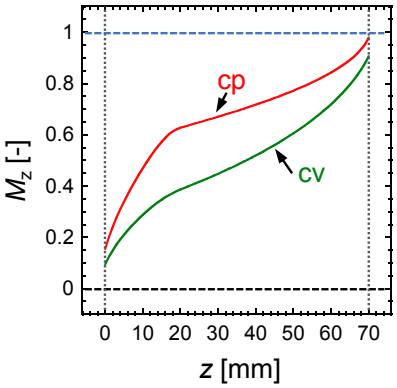

(b) transitions of theoretical Mach number

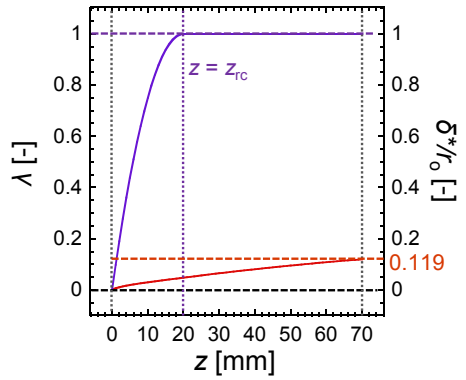

(c) transitions of theoretical λ and δ^*/r_o

Fig. 8 Transition of theoretical pressure with experimental pressure of Test 6 (a), transition of theoretical Mach number (b), and transition of chemical reaction progress λ and boundary thickness δ^* of constant-pressure calculation (c). The theoretical values are calculated under the same combustion conditions used in Test 6 (p_c = 252 kPa, Φ = 1.8).

https://doi.org/10.2514/1.J058322
AIAA JOURNAL, Vol. 58, No. 12, pp.5107-5116, December 2020

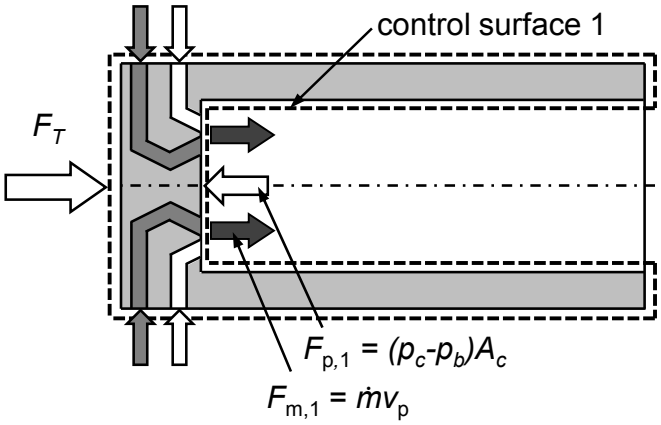

Fig. 9 Scheme of control surface 1, which was set on the surface of the RDE, including the injector plate surface.

https://doi.org/10.2514/1.J058322
AIAA JOURNAL, Vol. 58, No. 12, pp.5107-5116, December 2020

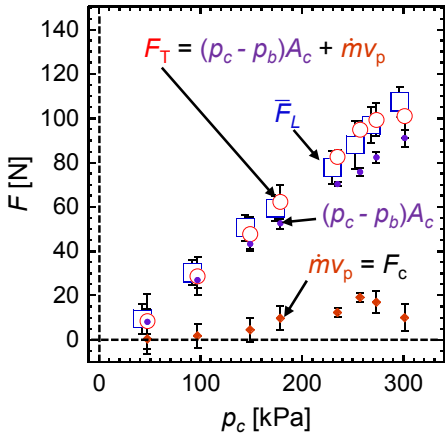

Fig. 10 Comparison of load cell thrust $\overline{F}_L$ and total thrust F_T of pressure thrust $(p_c - p_e)A_c$ and momentum thrust $\dot{m}v_p$. Both the pressure thrust and momentum thrust of F_T were measured on control surface 1. Note that pressure thrust, momentum thrust, and total thrust of F_T move by +5 kPa in the plot.

https://doi.org/10.2514/1.J058322
AIAA JOURNAL, Vol. 58, No. 12, pp.5107-5116, December 2020

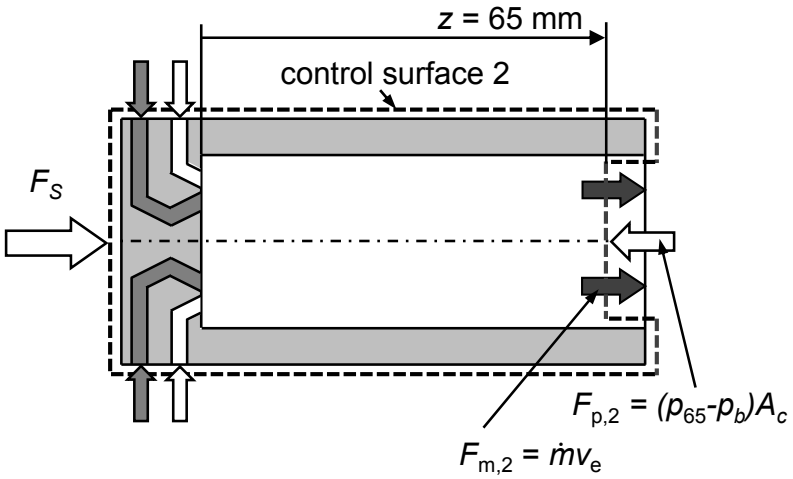

Fig. 11 Scheme of control surface 2, which was set to cover the RDE. The surface covers the exit surface of the RDE.

https://doi.org/10.2514/1.J058322
AIAA JOURNAL, Vol. 58, No. 12, pp.5107-5116, December 2020

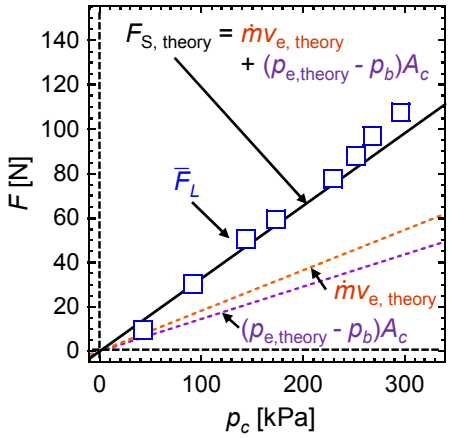

Fig. 12 Comparison of load cell thrust $\overline{F}_L$ and theoretical thrust $F_{S,\,theory}$ calculated on the assumption that exit flow is sonic flow. Pressure thrust $(p_{e,\,theory} - p_b)A_c$ and momentum thrust $\dot{m}v_{e,\,theory}$ are also plotted.

https://doi.org/10.2514/1.J058322
AIAA JOURNAL, Vol. 58, No. 12, pp.5107-5116, December 2020

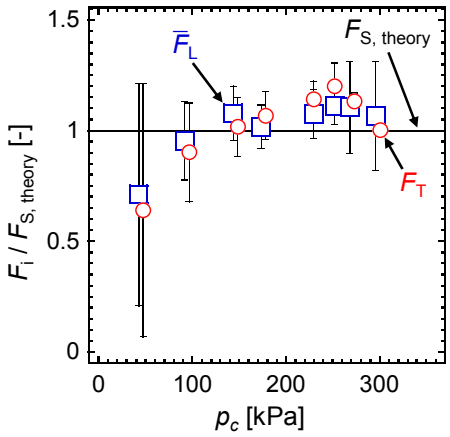

Fig. 13 Comparison of $\bar{F}_L$, F_T normalized by $F_{S,\,theory}$. Note that F_T move by +5 kPa in the plot.

https://doi.org/10.2514/1.J058322
AIAA JOURNAL, Vol. 58, No. 12, pp.5107-5116, December 2020

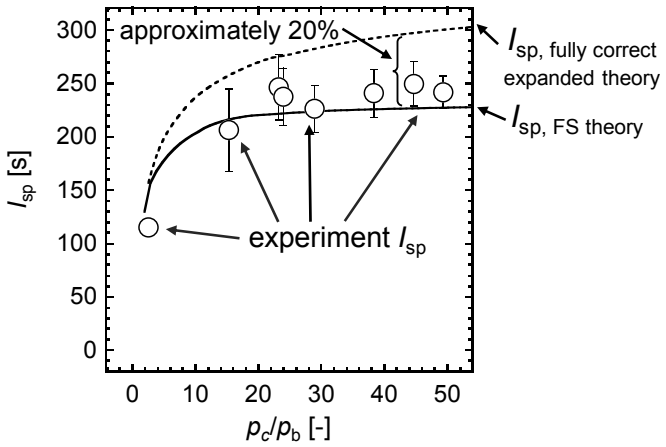

Fig. 14 Experimental I_{sp} of cylindrical RDE at various chamber pressures. $I_{sp,\ fully\ correct\ expanded\ theory}$ is defined as I_{sp} of the correct expansion from chamber pressure p_c ($\Phi = 1.8$) to back pressure p_b, and $I_{sp,\ FS\ theory}$ is defined as I_{sp} when the burned gas of chamber pressure p_c ($\Phi = 1.8$) accelerates to sonic flow. They were calculated by NASA-CEA [28].